2D Modelling with Linearized Integral Equations

Ulrich SCHMUCKER

Geophysikalisches Institut, Goettingen - D-37073, Germany

A reduced COPROD2 data set with response estimates at twenty sites for four periods (85 s to 683 s) is interpreted, using an iterative modelling scheme on the basis of linearized integral equations. Input data are the anomalous fields, here E_{ax} and B_{az} for E-polarisation, which are derived from the supplied impedances Z_{xy} and the magnetic transfer functions T_{zy}. Prior to 2D modelling a normal 1D reference model is introduced (here a 3-layer model) and an anomalous domain defined (here from zero to 40 km depth and 200 km in width). It is subdivided into M subdomains of constant anomalous conductivity.

The linearisation of the non-linear data functional is performed by approximating the internal field E_x within the anomalous domain. An iterative process is started with the normal field E_{nx} of the 1D reference model as internal field, gradually improving this first approximation. The evolving linear problem is solved by the least-squares method, adapting the data kernel with each iteration step better to the model which arises from the application of this kernel to the data. No Frechet derivatives of the data functional are involved and no starting model is required.

A first set of models is derived from MT data alone, a second set from combined MT/GDS data, increasing the number of subdomains from $M = 1$ to $M = 64$. It is found that with $M = 8$ (i.e. with 20×50 km^2 subdomains) the resolution power of the data is exhausted.

The resulting models have an almost uniform top layer and a deep-seated central region of reduced resistivity of 10 Ωm at 20 to 40 km depth. Further modelling studies show that a deep origin of the observed anomalies is indeed more likely than a shallow origin and that the modelling results do not depend significantly on the used periods. The mean residual (if only MT data are used) is greater than the data error and the individual residuals are not randomly distributed; both indicate that the data have not been exploited to their fullest possible extent. Forward modelling shows that the models are not in good agreement with B-polarisation impedances.

1. Data Selection and Description

From the total COPROD2 data set I decided to interpret a reduced set, comprising response estimates from twenty sites and four periods. *In strict adherence* to given instructions, the sites are from station PC5008 at -114 km to station PC5007 at $+120$ km, without the two in-between sites PC5405 and PC5305. The assigned periods for the reduced data set are 85, 171, 341, and 683 seconds.

The interpretation will be based mainly on the impedances Z_{xy} for *E*-polarisation for reasons which will become apparent later. At 683 s five impedance estimates and at 171 s one estimate have been marked as unreliable. They are not used. This leaves a total number of 74 apparent resistivities ρ_a and phases ϕ, or 148 real and imaginary parts of the impedance

$$Z_{xy} = \sqrt{\frac{\omega}{\mu_0} \rho_a} e^{i\phi}.$$

Separate confidence limits are listed for ρ_a and ϕ at an unspecified confidence level. They are used to define errors $\Delta\rho_a$ and $\Delta\phi$ for both quantities. Assuming that $\Delta\rho_a/2\rho_a$ and $\Delta\phi$ are equivalent

estimates for the relative error of $|Z_{xy}|$, the following common errors are assigned to the real and imaginary parts of Z_{xy}:

$$\Delta Z_{xy} = |Z_{xy}| \cdot \{\Delta\rho_a/2\rho_a + \Delta\phi\}/2.$$

The supplied response estimates refer to the locally observed horizontal magnetic field B_y and thus involve two anomalies: one for the electric field E_x (or the vertical magnetic field B_z) and one for B_y. The method to be used requires a separate treatment and presumes that the fields are referenced to the same normal fields E_{nx} and B_{ny} at all sites. This implies induction by a quasi-uniform source with the same normal structure $\sigma_n(z)$ extending on either side to infinity. For simplicity the normalisation will not be expressed explicitly, i.e. E_x stands from now on for the dimensionless ratio E_x/E_{nx}, B_y for B_y/B_{ny}, and B_z for B_z/B_{ny}.

Let Z_n denote the impedance E_{nx}/B_{ny} of the normal structure. Then the normalised electric field in terms of the locally referenced impedance is $E_x = Z_{xy}/Z_n \cdot B_y$. The input data for the 2D modelling process are not, however, these total fields, but only the differences $E_{ax} = E_x - E_{nx}$ and $B_{ay} = B_y - B_{nx}$ with the identity $B_{az} = B_z$. Obviously, they are direct expressions of the anomalous conductivity $\sigma_a = \sigma - \sigma_n$ to be found, when σ_n represent only the depth-dependent normal conductivity of the surrounding area.

Hence, for a given site and period the input datum and its error are

$$E_{ax} = \frac{Z_{xy}}{Z_n} \cdot (1 + B_{ay}) - 1, \quad \Delta E_{ax} = \frac{\Delta Z_{xy}}{Z_n} \cdot (1 + B_{ay}) \qquad (1)$$

for the anomalous electric field and

$$B_{az} = T_{zy} \cdot (1 + B_{ay}), \quad \Delta B_{az} = \Delta T_{zy} \cdot (1 + B_{ay}) \qquad (2)$$

for the anomalous vertical magnetic field with $T_{zy} = B_z/B_y$. Again, E_{ax} stands for E_{ax}/E_{nx}, B_{ay} and B_{az} for B_{ay}/B_{ny} and B_{az}/B_{ny}.

The COPROD2 data set provides estimates for Z_{xy} and T_{zy}, but has no information on B_{ay} or at least on the variable horizontal field with respect to some fixed reference station. In principle B_{ay} could be derived from B_{az} (and thereby from T_{zy}) by a Hilbert transformation (as they are components of a 2D potential field of internal origin). The large uncertainties in the estimates of T_{zy}, and the fact that the COPROD2 profile ends where T_{zy} has its peak value, make such a determination unrealistic. Therefore theoretical model values B_{ay}^* will be used to define the input data in terms of observables as follows:

The iterative process is started with zero anomalous conductivity, i.e. with $B_{ay}^* = 0$. The model found in the first iterative step supplies a first approximation for B_{ay}^* which yields, when inserted into Eqs. (1) and (2), modified data for the second iteration and so on. In this way the set of input data and their errors depend not only on the adopted 1D model (in the case of E_{ax}), but also on changing 2D models which evolve during the iterative process.

Under the given circumstances this problematic reshaping of the input data by models derived from them is unavoidable. It may be responsible for certain peculiarities which were observed in the iterative process and which were not encountered when the original data were already properly normalized. Besides the mere necessity to recast the supplied data in the described form, this has also definite benefits: Firstly, dimensionless quantities are interpreted which are of comparable size for all three components and all periods, provided that the top layers are without sharp conductivity contacts. (Otherwise, at sufficiently short periods the anomalous magnetic fields disappear while the anomalous electric fields become large, when the impedances merge into their locally determined and thus greatly variable 1D responses.) In this respect the COPROD2 data were taken under most favourable conditions. At short periods below 10 s the ρ_a values almost uniformly lie between 2 Ωm and 4 Ωm.
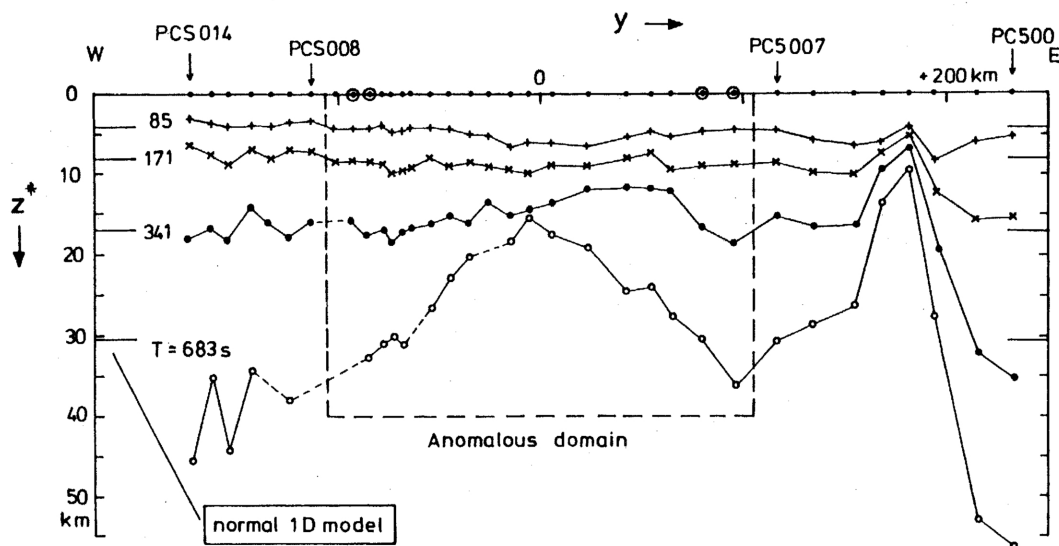
Fig. 1. Penetration depths z^* of E-polarisation along the COPROD2 profile at 35 sites and for the four periods of interpretation. Their deviation from the 1D normal level indicates zones of anomalous conductivity, here a well conducting zone in the centre and a transition to low conductivities at the eastern end beyond 200 km. 1D modelling is carried out at the encircled sites, 2D modelling within the shown anomalous domain.

In the reduced COPROD2 data set the *rms* anomalous field amplitudes are indeed of comparable size, namely

$$0.18 \quad \text{for} \quad E_{ax} \quad \text{and} \quad 0.13 \quad \text{for} \quad B_{az}.$$

The quoted values are the squareroots of $\langle |E_{ax}|^2 \rangle$ and $\langle |B_{az}|^2 \rangle$, averaged over all twenty sites and all four periods. Their dependence on the adopted model of reduction is negligible.

2. The 1D Normal Model

The search for a suitable normal model $\sigma_n(z)$ is guided by a visual inspection of the supplied data: Fig. 1 shows the depths $z^* = Im\{Z_{xy}\}/\omega$ for four selected periods along the entire CO-PROD2 profile. This depth of a perfect substitute conductor (to explain the out-of-phase part of the impedance) images the variable depth of penetration from site to site and period to period. Note that no cross-overs occur, i.e. z^* increases at all sites with increasing period. This applies also for most periods not shown and gives a good testimony for the quality of the supplied data.

In detail: The z^* curve for 683 s ascends smoothly from a mean depth of 40 km in the far west to a minimum of 15 km in the center, indicating here a presumably deep-seated body of low resistivity. At shorter periods the z^* minimum is less pronounced and shifted eastwards. At the eastern end a second sharp z^*-minimum occurs in all periods, followed by a steep descent. Hence, a narrow low resistivity zone lies here next to a high resistivity region of unknown extent toward east.

The transfer functions T_{zy} in Fig. 2 support this interpretation: westward of the center a minimum of their real parts and eastward a maximum with a reversed trend in the imaginary parts. The proposed transition to an extended high resistivity region beyond the most eastern station could explain equally well the strong positive anomaly of the real part at the last three sites. It will be difficult, however, to develop from the available data a conclusive model for the
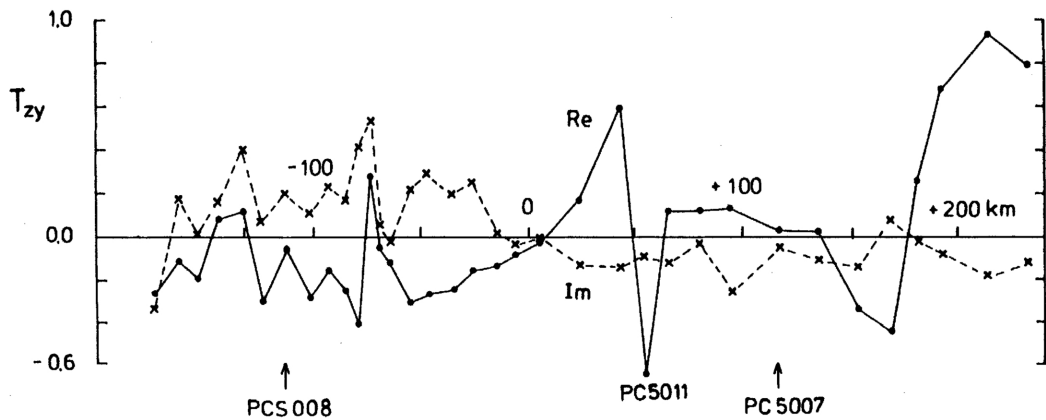
Fig. 2. Magnetic variation anomalies at 683 s period along the COPROD2 profile. In the center and at the eastern end they are consistent with indications by z^* in Fig. 1 for zones of anomalous conductivity.
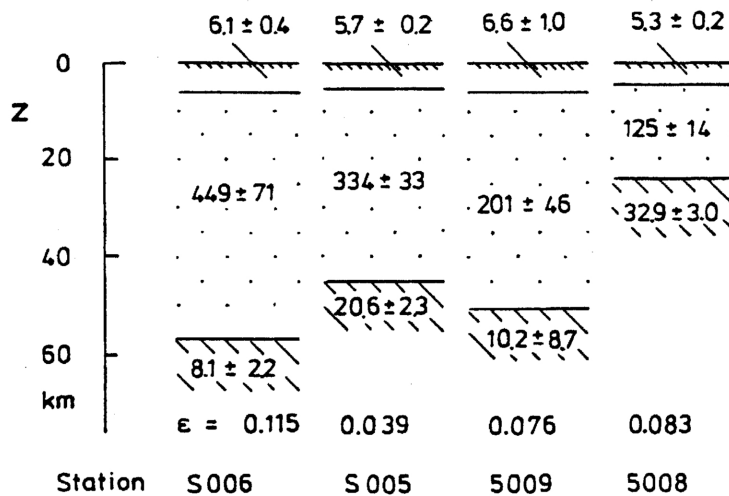

Fig. 3. 3-layer models derived from Z_{xy} impedances at the encircled sites of Fig. 1, using four periods. The residuals ϵ refer to the fit of the squared logarithmic impedance. Hence, ϵ represents the mean relative misfit of apparent resistivity or alternatively the mean phase misfit, multiplied by two, in angular measure.

eastern section of the profile. The exclusion of all stations beyond station PC5007 by using the reduced data set is therefore well founded and focuses the interpretation on the well documented structure in the center.

Figure 1 shows at either end of the reduced profile two specially marked stations. Their Z_{xy} impedances have been used to develop a 1D model as normal reference for the subsequent 2D interpretation. Even though only estimates of four periods are involved, the Ψ-algorithm of interpreting 1D data allows a subdivision into three layers as shown in Fig. 3 (for a short description of this algorithm see LARSEN, 1975, p. 33).

The selected sites yield essentially similar models: A conducting top layer of about 5 km
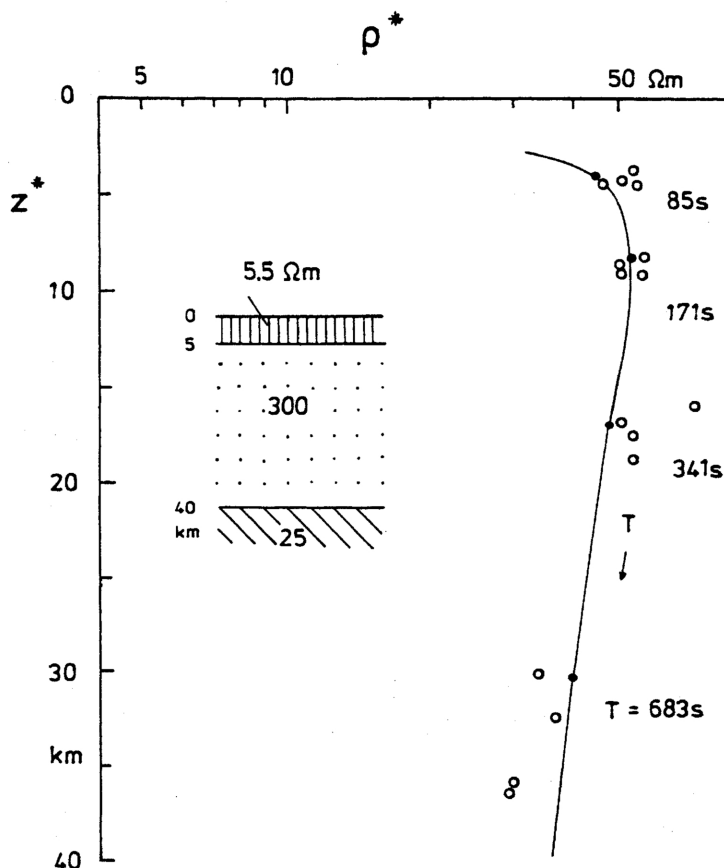
Fig. 4. $\rho^*(z^*)$-curve for the shown 3-layer model of the chosen normal structure. Filled circles on this curve refer to the four periods of interpretation, open circles to empirical estimates of the impedance Z_{xy} at these periods and the four sites used for 1D interpretation.

thickness with 5 Ωm–6 Ωm and a conducting lower halfspace of 10 Ωm–30 Ωm, separated by a poorly conducting second layer of 20 km–40 km thickness. These models have been combined into the following 3-layer model:

   5.5 Ωm to 5 km depth, then 300 Ωm to 40 km depth and 25 Ωm below 40 km.

Figure 4 shows the theoretical $\rho^*(z^*)$-curve for this model together with empirical estimates from the four sites and the four periods.

3.   The Method of 2D Interpretation

Its basis are integral equations which utilize Green's functions to connect the anomalous field at a field point $\underline{r}$ to the total field at source points $\underline{r}'$, both position vectors lying in the (y, z) plane. This plane is perpendicular to the strike directions of a 2D structure $\sigma(y, z) = \sigma_n(z) + \sigma_a(y, z)$. In the case of E-polarisation the integral equation for the anomalous electric field is

$$E_{ax}(\underline{r}) = -i\omega\mu_o \int_A \sigma_a(\underline{r}') \cdot G(\underline{r}, \underline{r}') E_x(\underline{r}') dA \qquad (3)$$

with $G(\underline{r}, \underline{r}')$ as Green's function for the adopted normal structure. Differentiation with respect to the fieldpoint coordinates leads to integral equations for the anomalous magnetic field:

$$B_{ay}(\underline{r}) = \mu_0 \int_A \sigma_a(\underline{r}') \cdot \partial G(\underline{r}, \underline{r}')/\partial z \cdot E_x(\underline{r}') dA,$$
$$B_{az}(\underline{r}) = -\mu_0 \int_A \sigma_a(\underline{r}') \cdot \partial G(\underline{r}, \underline{r}')/\partial y \cdot E_x(\underline{r}') dA. \tag{4}$$

The integrations are over the anomalous domains of non-zero $\sigma_a(\underline{r}')$, which must be bounded.

Let the field points be the surface points of observation and any of the anomalous fields at these points be the data. Green's function and the normal field $E_{ny}(z') = E_x(\underline{r}') - E_{ax}(\underline{r}')$ at the source point depth are derivable from σ_n and thus known. Unknown, and to be determined from the data, is σ_a. Because E_{ax} depends on the total conductivity, it depends also on σ_a and the stated inverse problem is non-linear.

Suppose this non-linearity is weak in the sense that E_x is not too far from its normal value E_{nx}. Then an iterative process can be started by substitution of E_{nx} for E_x in Eqs. (3) and (4) which linearizes the functional connecting data and model. Solving the resulting system of linear equations yields a first approximation $\sigma_a^{(1)}$ for σ_a, from which follows by forward modelling a first approximation $E_{ax}^{(1)}$ for the anomalous field. The linear system is solved again with $E_{nx} + E_{ax}^{(1)}$ for E_x, which generates second approximations $\sigma_a^{(2)}$ and $E_{ax}^{(2)}$. The process is repeated until it converges towards a stable solution in the following sense:

Let ϵ be the mean residual of the least-squares solution $\sigma_a^{(j)}$ as defined in Eq. (8) for the j-th iteration, i.e. with the approximation $E_{nx} + E_{ax}^{(j-1)}$ for E_x in data kernel. Let ϵ^* be the same mean residual, but now as model misfit residual with the correct internal field $E_{nx} + E_{ax}^{(j)}$ for the model $\sigma_a^{(j)}$. Provided that the process converges, the difference between these two residuals should gradually decrease, when the change in the internal field from iteration to iteration and thereby the change of the data kernel abate.

This convergence has been observed with no exception, when interpreting the reduced CO-PROD2 data set. Here the iterative process was terminated as soon as ϵ^* deviated less than 10^{-4} from ϵ, which mostly required five to six iterations, but never more than nine iterations.

Stability and convergence of the described method will depend on how well E_{nx} approximates the total field within the anomalous domain. In the models of this study E_x deviates in amplitude in general less than 25 percent from E_{nx}, even though at critical points and periods the ratio $|E_{ax}/E_{nx}|$ may reach 0.8. Table 1 illustrates in the case of model M8 in Fig. 5, how in a sequence of eight iterations the residuals ϵ and ϵ^* approach each other and how the solutions converge toward stable anomalous conductivities. The selected subdomains are those with the greatest deviations from the normal structure. The entries, which begin for completeness with those for no anomaly, show that the quoted threshold is reached after six iterations and that the model parameters are stable afterwards. These results are representative for all other calculations.

Since each iteration generates a new model from the *original* data, the here described methods differs substantially from those in which, as in the gradient method, models are gradually improved to fit the data. Here the data kernel is improved in its adaption to the models which it produces when applied to the data. In Electrical Engineering, I was informed, this procedure is known as "Perturbed Born-approximation". In the context of EM induction it has been introduced by WEIDELT (1978) to interpret a B_{az}-anomaly of geomagnetic variations in Northern Germany by 2D structures.

For discretisation of the problem the anomalous domain is divided into M uniform subdomains A_m. Their anomalous conductivities define an equal number of discrete model parameters x_m. Let the datum y_n be the real or imaginary part of an anomalous field at a certain site and period, yielding N data for $N/2$ complex response estimates of E_{ax}, B_{ay}, B_{az} or any combination

M1
(0.1439)

-105   +95 km

5.5	5.1 ± 0.0	5.5
	58 ± 1	

40 km   25 Ωm

M2
(0.1189)

5.4 ± 0.0
191 ± 17
12.5 ± 0.4

M4
(0.1187)

5.5 ± 0.0	5.3 ± 0.0
359 ± 68	98 ± 9
17.6 ± 0.9	8.5 ± 0.5

M8
(0.0966)

5.5	5.3	4.9	5.5
368 ±76	101 ±9	39 ±2	231 ±50
93 ±11	13.7 ±0.3	11.7 ±0.4	35.2 ±3.7

M16
(0.1117)

5.5	5.6	5.3	5.5
423	4480	93	433
228	28	20	71
104	23	19	51
78	26	24	51

M32
(0.1179)

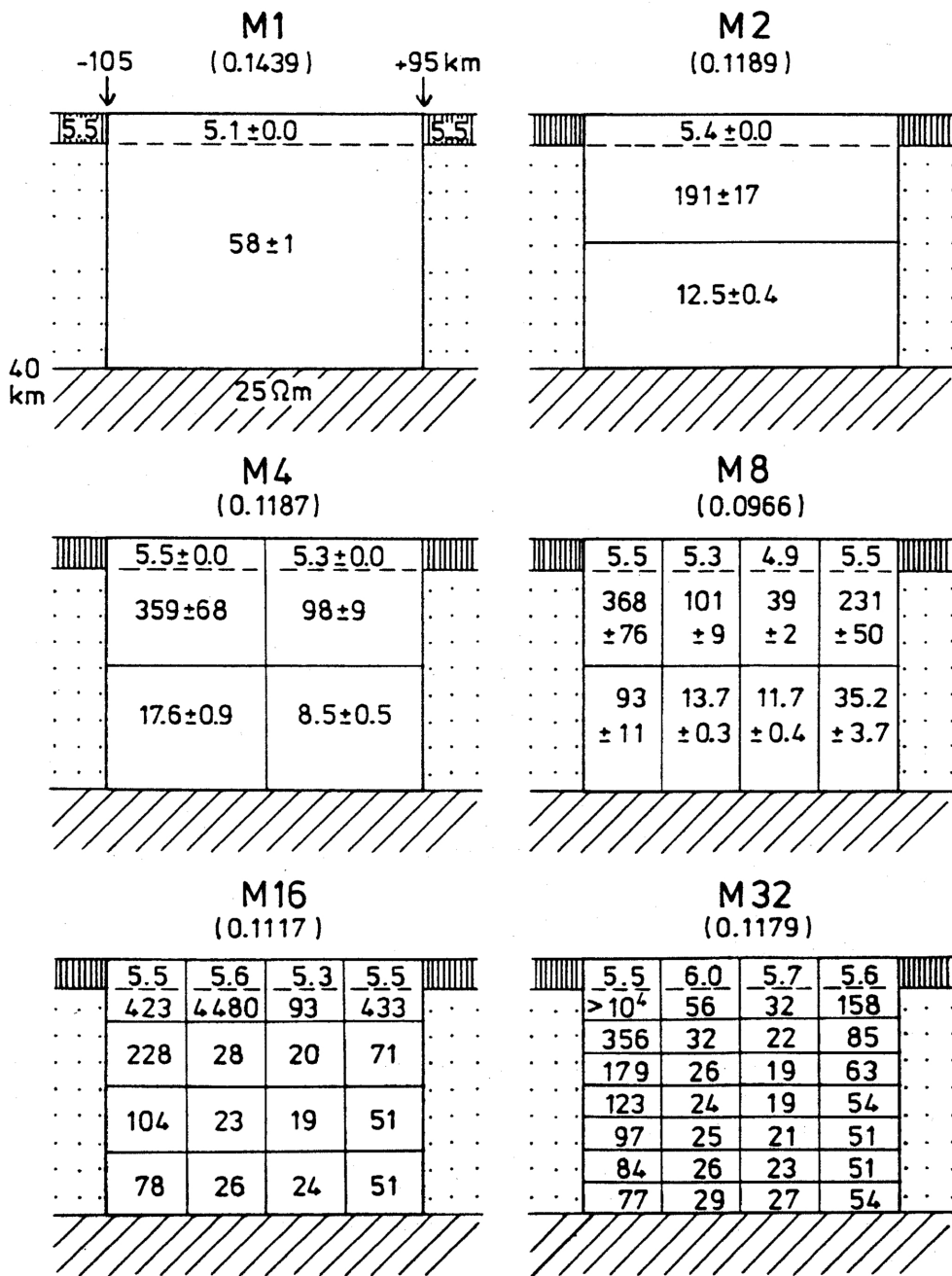| 5.5	6.0	5.7	5.6
>10^4	56	32	158
356	32	22	85
179	26	19	63
123	24	19	54
97	25	21	51
84	26	23	51
77	29	27	54

Fig. 5. 2D models derived from Z_{xy} impedances at twenty sites and four periods. The same 1D normal model as shown for model M1 applies to all other models. Numbers are subdomain resistivities with errors, in Ωm. Residuals ϵ in parenthesis. Cf. Table 2.

Table 1. Iterative process of MT data interpretation with $N = 148$ data and $M = 8$ model parameter.

ϵ	:	least squares mean residual;
ϵ^*	:	model misfit mean residual;
$\sigma_a(i,j)$	:	anomalous conductivity of subdomain in i-th row and j-th column of (2×4) model, in S/m;
$\rho(i,j)$	:	subdomain resistivities, in Ωm.

Iteration	ϵ	ϵ^*	$\sigma_a(1,1)$	$\sigma_a(2,3)$	$\rho(1,1)$	$\rho(2,3)$
	0.18880	0.00000	0.00000	0.00000	300	300
1	0.12830	0.11924	−0.00240	0.09191	1071	10.50
2	0.10336	0.10315	111	9215	450	10.47
3	0.09758	0.09854	81	8493	396	11.33
4	0.09688	0.09717	59	8272	364	11.62
5	0.09684	0.09691	62	8220	368	11.69
$6^{1)}$	0.09683	0.09684	62	8209	368	11.71
7	0.09683	0.09683	62	8208	368	11.71
8	0.09683	0.09683	62	8208	368	11.71

[1)] last iteration in deriving model M8.

of them. Then the data kernel in the linear system

$$y_n = \sum_m g_{nm} x_m + \delta y_n \qquad (n = 1, 2, \ldots, N) \tag{5}$$

for the j-th iteration and the real part of E_{ax} as datum is, as seen from Eq. (3),

$$g_{nm} = Re \left\{ -i\omega\mu_0 \int_{A_m} G(\underline{r}, \underline{r}') E_x^{(j)}(\underline{r}') dA_m \right\};$$

$\underline{r}$ is the position vector of the fieldpoint, where the datum has been taken. In the case of B_{ay} or B_{az} the respective derivative of the Green's function is to be used according to Eqs. (4). For the imaginary part of the anomalous field, the data kernel will be the negative real part of the integral expression. No weights are used for the data y_n and thereby the residuals δy_n are unnormalized with respect to the empirical data errors ΔE_{ax} or ΔB_{az}.

The least-squares solution which minimizes the sum

$$S = \sum_n \delta y_n^2$$

may require some stabilisation in case of oscillating models x_m. It is achieved by adding Marquardt's α^2 to the diagonal elements of the normal equations matrix. Let h_{mn} be an element of the resulting generalized inverse matrix

$$H = (G^T G + \alpha^2 I)^{-1} G^T \tag{6}$$

of the data kernel matrix $G = (g_{nm})$. Then the anomalous conductivity of the k-th subdomain and its errors are found from

$$\overline{x}_k = \sum_n h_{kn} y_n \qquad \text{and} \qquad \Delta \overline{x}_k^2 = \sum_n h_{kn}^2 \Delta y_n^2, \tag{7}$$

the thus defined mean squared residual from

$$\epsilon^2 = S/(N - M) = \left(\sum_n y_n^2 - \sum_m x_m \sum_n g_{nm} y_n - \alpha^2 \sum_m x_m^2 \right) /(N - M). \tag{8}$$

In deriving the model parameter errors $\Delta \overline{x}_k$ it has been assumed that the data errors are uncorrelated.

For $\alpha > 0$ the resulting model is a smoothed model, in which a resolution matrix $A = HG = (a_{km})$ connects the derived smoothed model parameter to those of the linear system:

$$\overline{x}_k = \sum_m a_{km} x_m. \qquad (9)$$

The integral equation for B_x in case of B-polarisation differs in two aspects: It is quasi-linear in respect to the *anomalous resistivity*

$$\rho_a = -\sigma_a \cdot \rho / \sigma_n,$$

rather than the anomalous conductivity, and it is more complicated because additional integrations along the boundaries of uniform subdomains are required. In fact, the anomalous fields B_{ax} and E_{ay} are mainly determined by these line integrals, when the impedance Z_{yx} is not too close to its locally determined 1D value and the effect of electric charges on domain boundaries predominant. In any case, the integral equation can be linearized in the same way. Details can be found in SCHMUCKER (1992).

Tests with synthetic data have shown that the iterative process to derive ρ_a from E_{ay} is less stable than the process to derive σ_a from E_{ax} in case of E-polarisation. Furthermore, because ρ_a and σ_a are not linearly related, B-polarisation and E-polarisation data cannot be combined into a single data set. For these two reasons the COPROD2 data for B-polarisation are not considered, even though forward calculations will be performed to see, whether the derived models for E-polarisation generate acceptable B-polarisation responses.

4. 2D Modelling Results

It should be observed that these results are subject to two major a priori decisions (i) on the shape and position of the anomalous domain and (ii) on the 1D normal model outside that domain. It has been stated already that z^* does not exceed anywhere 40 km and that this may be regarded as the maximum depth reached by the downward diffusing fields at the longest period. Therefore the anomalous domain has been bounded at 40 km depth and laterally at -105 km and $+95$ km as indicated in Fig. 1.

The choice of a suitable 1D normal model has been discussed in Section 2. The programs also permit varying the 1D normal model as part of the iterative 2D modelling process. Suppose a 2D model has been found, then 2D corrections are applied to the impedances at those sites, which were used to establish the 1D model. The 1D modelling is repeated with 2D-corrected impedances, yielding a new and better adapted normal model. This option has not been used, however, and all models refer here to the same normal model as given at the end of Section 2 and shown in Fig. 4.

The anomalous domain of 40×200 km^2 is now subdivided into an increasing number of subdomains up to $M = 64$ as shown in Fig. 5. Input data are 74 complex-valued anomalous field estimates E_{ax} with their errors as discussed in Section 1. The resulting subdomain anomalous conductivities σ_a and their errors are converted for convenience into subdomain resistivities and their errors as displayed also in Fig. 5. It should be noted that this conversion involves the adopted normal conductivity σ_n, which changes at 5 km depth. Therefore, even when σ_a is identical above and below that depth, ρ will be different.

Table 2 lists for each model in the first column the mean data residuals of Eq. (8) to express the overall misfit between input and model data. Then follow the *rms* residuals of the impedance,

Table 2. Residuals for 2D models from MT data ($N = 148$).

Model	M	$\epsilon(y)$	$\epsilon(Z_{xy})$	$\epsilon(\rho_a)$	$\epsilon(\phi)$	α
M 0	0	0.1888	0.1167 km/s	9.2 Ωm	8.8 degrees	0
M 1	1	0.1439	0.0907	6.0	8.8	0
M 2	2	0.1189	0.0762	5.4	6.1	0
M 4	4	0.1187	0.0741	5.5	5.9	0
M 8	8	0.0966	0.0566	3.8	6.4	6
M16	16	0.1117	0.0620	4.3	6.9	6
M32	32	0.1179	0.0609	4.3	6.8	4
M64	64	0.1407	0.0616	4.4	6.9	3

the apparent resistivity and phase, dividing the respective sums of squared individual residuals by $(N - 1)$, not by $(N - M)$. The last column lists the stabilizing constant α of Eq. (6).

The entries begin with model M0 which has no anomalous domain at all and ϵ is simply the *rms* amplitude of the input data. The other residuals express the differences between the observed and the calculated response data for the adopted normal 1D model. Figure 1 shows how the empirical z^* estimates deviate from their indicated normal levels.

It follows model M1 with an undivided anomalous domain. The residual for E_{ax} is clearly reduced. More progress is made, when this domain is subdivided in model M2 into an upper and lower half. The residual is now 2/3 of its initial value for no anomaly. An additional vertical boundary in model M4 has virtually no effect.

Obviously a finer structuring is needed in the horizontal direction. Two more vertical boundaries and thus a subdivision into eight domains brings in model M8 the residual further down. It appears that this is the best achievable fit since further subdivisions into 16, 32, and 64 domains yield no improvements. The increase of ϵ from $M = 16$ onwards reflects mostly the decreasing number $(N - M)$ of "degrees of freedom", while the sum S of squared data residuals is nearly unchanged. All these models are shown in Fig. 5 except M64. Hence, a subdivision into domains of 20×50 km^2 cross-section seems to reflect the spatial resolving power of the data.

The failure to improve the fit, at least marginally, beyond $M = 8$ may reflect to some extent the uncontrolled use of a stabilising constant α simply to avoid negative conductivities, discussed below. On the other hand, the statement about the resolving power will be strengthened also by considering the spread of the resolution kernel. Supporting evidence comes also from the spread of eigenvalues λ_j^2 of the $G^T G$ matrix, which justifies the performed stabilisation regardless of other considerations. In fact, for $M \geq 8$, α^2 corresponds in size to the fourth eigenvalue and thus yields $\lambda_j^2/(\alpha^2 + \lambda_j^2) \approx 0.5$ as weight of λ_j^{-1} for $j = 4$, i.e. the smoothed model $\overline{x}_k$ is determined essentially by the first eight eigenvalues regardless of the chosen number of subdomains. Model accuracy in correspondence to data errors should be also indicative for model resolution. The derived errors of subdomain resistivities are so small, however, as to justify all models including M64.

Turning now to the residuals of the original data (Z_{xy}, ρ_a, ϕ), similar improvements of the fit are observed by 2D modelling. It should be remembered, however, that impedances at four out of twenty sites have been used to define the adopted 1D model. It has for Z_{xy} the quoted residual of 0.1167 km/s, while the *rms* amplitude of Z_{xy} is 0.45 km/s. The best fitting 2D models have residuals of about 0.06 km/s.

Disturbing is the fact that the best possible fit is inadequate, if it were limited by random data errors, i.e. the minimum mean residual of 0.0966 is in excess of the mean data error ΔE_{ax} of Eq. (1), which is 0.04. The discrepancy implies (apart from the possibility of systematic data errors) that the models have an inherent deficiency to explain the data. For instance, the

adopted 1D model could be an inadequate representation for the surrounding deep structure, or the anomalous domain could be not large enough, or simply 3D effects. Various tests have shown that neither an enlarged anomalous domain nor different 1D normal models can bring ϵ nearer to ΔE_{ax}. The real cause of the discrepancy remains therefore unresolved.

This limits the actual meaning of the model parameter errors as displayed in Fig. 5. Their derivation presumes random and independent data errors. The true uncertainties should be greater. It is interesting to note that the quoted errors do not increase markedly for models with more subdivisions, indicating that the linear problems involved remain well overdetermined, even when M is increased up to 64. The reason for dampening the solutions by Marquardt's α is not instability, but the fact that negative resistivities appear during the 2D modelling process.

Even though there may be better ways to ensure solutions with $\sigma_a > -\sigma_n$, I have decided to use in such cases a generalized inverse of the data kernel as described in Section 3 (Eq. (6)). The smallest possible α to produce positive resistivities in all subdomains is used; it is found by trial and error. A preferable orientation on data error (to produce a mean residual ϵ of the same size as the mean data error) is not possible for reasons given above. It is also uncertain to which degree the linearisation of a non-linear inverse problem is involved, when at the shortest periods E_{ax} is not too far from unity, or the reformulation of the input data during the iteration process (cf. Section 1).

After considering model fit and model accuracy the third quantity to be studied is model resolution. Up to $M = 4$ no dampening of the solution is necessary and the resolution is "perfect". To demonstrate the degree of averaging from $M = 8$ onwards, Fig. 6 displays the elements of the resolution matrix (a_{km}) of Eq. (9) for one specific row, referring to a subdomain near the center of the anomalous domain. For $M = 8$ the resolution is still nearly perfect, supporting the supposition from above that this number agrees to the resolving power of the input data.

For $M = 16, 32, 64$ the derived model parameters are averages over an increasing number of domains, but basically of those which are above and below the target domain. The resolution with regard to depth appears in this way as poorer than the resolution in horizontal distance. But here the aspect ratio of height to width of the domains should be noted, which is 1:5 for $M = 4$, 16, 64. The cross-section of the anomalous domain to the right illustrates for one specific model the changing resolution with position of the target domain. The displayed diagonal elements of the resolution matrix clearly demonstrate the vanishing resolution with depth.

Partially successful have been attempts to include the magnetic variation anomaly B_{az} into the modelling process. Table 3 lists the obtained residuals for models of the same design as model $M8$, interpreting now 146 complex data. (The strongly deviating T_{zy} estimates at stations PCS004 and PC5011 are omitted.) The first quoted residual is that for the combined data, then follow the rms residuals for the anomalous electric and the anomalous vertical magnetic fields. The resulting models are not shown. They are similar to the M8 model in Fig. 5.

By combining in this way MT and GDS input data, the fit for E_{ax} is clearly downgraded

Table 3. Residuals for 2D models from combined MT and GDS data (M=8 and 64).

1. MT data from 20 and GDS data from 18 sites
2. only GDS data from 18 sites
3. MT data from 20 and GDS data from 12 sites

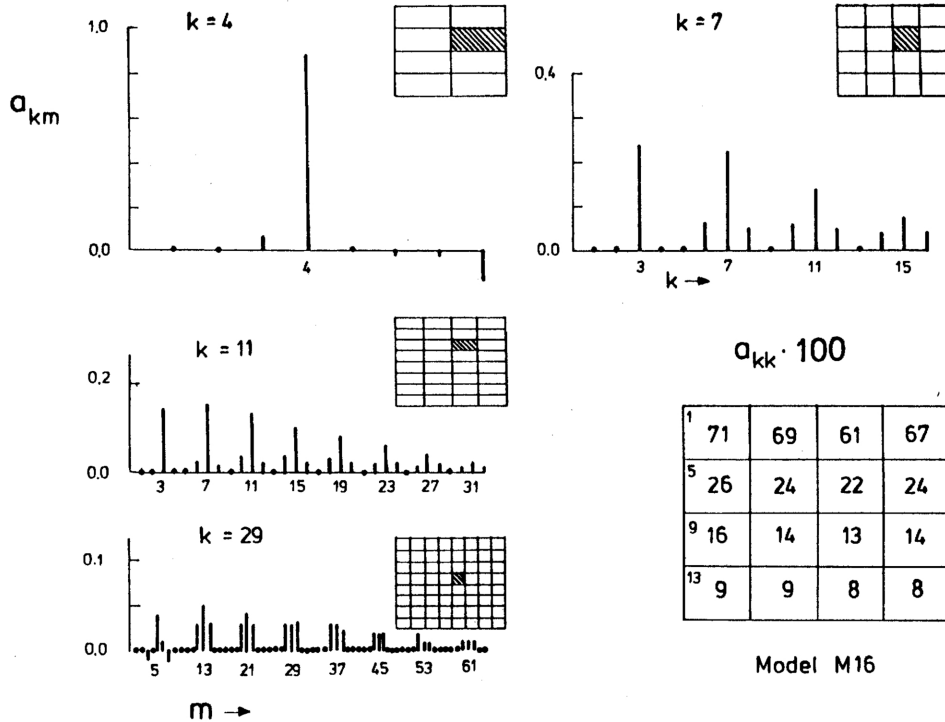| Model	N	$\epsilon(y)$	$\epsilon(E_{ax})$	$\epsilon(B_{az})$	$\epsilon(Z_{xy})$	$\epsilon(\rho_a)$	$\epsilon(\phi)$
M8–1	292	0.1259	0.1272	0.1210	0.0789 km/s	5.6 Ωm	7.3 degrees
M8–2	144			0.1249		7.0	8.8
M8–3	244	0.0979	0.0909	0.1041	0.0543	3.5	6.6
M64–3	244	0.1273	0.1079	0.1115	0.0625	4.3	7.3

Fig. 6. Resolution of models M8 to M64, Table 2 and Fig. 5. Shown are for each model the elements a_{km} of the resolution matrix Eq. (9) for target domain number k as indicated by shading in the schematic model cross–sections. Numbering of domains is from left to right, starting in the top row. The vertical bars in the four diagrams are the resolution elements for $m = 1, 2, \ldots, M$. For $m \neq k$ they indicate the degree of averaging over adjoining domains. With increasing number of subdivisions this averaging increases so as to give all models about the same spatial resolution. Bottom right: Diagonal elements of the resolution matrix for each subdomain in case of model M16, demonstrating the decrease in resolution with depth.

when compared to the fit which can be achieved with MT data alone. If only GDS data are used, then the misfit for B_{az} remains nearly as large as when no 2D modelling is performed and the residual is 0.1297 (model M8–2). A more satisfactory interpretation of combined MT/GDS data is possible, however, when sites with erratic and most badly determined T_{zy} estimates are omitted.

Thus, a new set of input data is formed with the MT data from all 20 sites as before, but with GDS data from only 12 sites, i.e., from station PC503 at −65 km to PC5009 at 80 km without station PC5011. In this way that GDS data section is retained, which appears to be most consistent with MT data as outlined in Section 2.

The resulting model M8–3 (shown in Fig. 9) provides not only the expected better fit for B_{az}, but has also slightly smaller residuals for E_{ax} and Z_{xy} than model M8 from MT data alone. The same applies to model M64–3 with 64 subdivisions. Hence, this data combination yields models which explain the COPROD2 data better than any other so far derived model.

Further calculations concern the question, whether the data could be explained equally well by a *reduced* anomalous domain, comprising either (sedimentary) top layers or alternatively the (crystalline) crust below them. The reduced domains are subdivided into $M = 8$ subdomains, their vertical extent is from 0 to 5 km for the top model M8–T and from 5 to 35 km for the deep model M8–D. Again only the anomalous electric fields E_{ax} are used as input data.

Both alternatives lead to acceptable model solutions, as is seen from Table 4, but the fit to these identical data is clearly worse for the top model. In fact, the deep model, with $\epsilon = 0.0910$, produces one of the smallest residuals. It is not shown because its subdomain resistivities are essentially the same as those of model M8 from 5 km on downward. The conclusion is therefore that an optimum interpretation of the COPROD2 impedances in E-polarisation requires a deep structure of variable conductivity, at least for the considered sites and periods.

In two additional models of the same design, named M8–T* and M8–D*, the excluded spaces below and above 5 km depth are filled with previously derived variable resistivities. They are kept unchanged during the subsequent modelling process. For the top model the deep structure is from model M8, for the deep model the top structure is from the resulting new top model M8–T*. With this modification, as to be expected, the top model also yields an almost optimum fit, while the deep model M8–D* has the best fit of all models. This model is the one reproduced in the introductory paper by JONES (1993).

A final series of calculations studies the influence that the period selection might have. Two new data sets are formed of six periods each. The first set comprises all available periods from 341 s to 909 s, of which three have been used before. (The two longest periods beyond 909 s are virtually without reliable impedance estimates.) This long period set generates, with $M = 8$, subdivisions model M8–L which reproduces model M8 within error limits. Only the central low resistivity anomaly has, in model M8–L, even more reduced resistivities, namely in the two central subdomains at the bottom 10.5 ± 0.2 Ωm and 9.9 ± 0.2 Ωm in place of 13.7 ± 0.3 Ωm and 11.7 ± 0.4 Ωm for model M8. The residual of model M8–L is greater than that for model M8, but in relation to the increased residual of no anomaly, which is now 0.2093, indicates a comparable reduction in variance by 2D modelling.

The second set is composed of the adjoining short periods from 21 s to 114 s, including the 85 s period of the old set. Noting that the penetration depths z^* hardly exceed 7 km anywhere; it is therefore not surprising that no stable solution can be found if the anomalous domain extends downward to 40 km. Thus, model M8–S derived from the second set is restricted to the upper

Table 4. Residuals for further 2D models from MT data (M=8).

T	: top anomalous domain (0 to 5 km)
T*	: top anomalous domain and preset resistivities from 5 to 35 km
D	: deep anomalous domain (5 to 35 km)
D*	: deep anomalous domain and preset resistivities from 0 to 5 km
L,S	: long or short period data
LS	: long and short period data

Model	N	$\epsilon(E_{ax})$	$\epsilon(Z_{xy})$	$\epsilon(\rho_a)$	$\epsilon(\phi)$		α
M8–T	148	0.1307	0.0772 km/s	4.3 Ωm	11.7	degrees	1.0
M8–D	148	0.0910	0.0538	4.8	7.9		6
M8–T*	148	0.0860	0.0497	4.2	9.8		0.75
M8–D*	148	0.0809	0.0456	3.3	5.3		4
M8–L	214	0.1047	0.0553	4.9	6.9		6
		(0.2093)	(0.1200)[1]				
M8–S	240	0.0875	0.0794	1.3	6.7		0
		(0.1053)	(0.0938)				
MS–LS	454	0.1073	0.0727	4.4	7.0		14
		(0.1628)	(0.1069)				

[1] residuals of no anomaly.

5 km (with $M = 8$ subdomains). The apparently small residual of 0.0875 should be compared, however, to the residual 0.1053 for no anomaly, i.e. at short periods the 2D modelling barely improves the fit over that obtained already with a 1D model.

Combining the two data sets to a single data set of twelve periods (from 21 s to 901 s) gives a final model M8–LS. Its fit is reasonably good, i.e. $\epsilon = 0.1073$ vs. 0.1628 for no anomaly. The model shows all the characteristics of model M8 except that the resistivity contrasts in the upper part are somewhat smaller, and those in the lower part somewhat larger, than in model M8. This corresponds to the conclusions from the long-period data.

Data from the remaining COPROD2 sites have been examined, but no results are presented. The data of the western section (site PC5014 at −174 km to PC5009 at −124 km) reveal a rather featureless deep structure. In contrast, those of the eastern section (site PC5006 at 135 km to
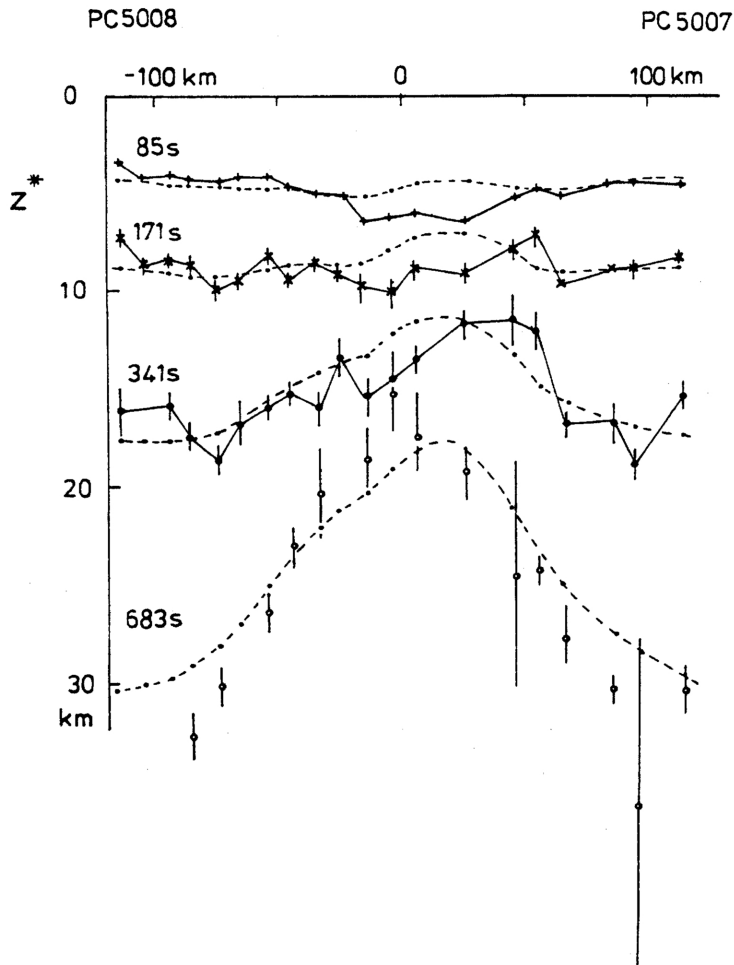
Fig. 7. Penetration depths z^* for the periods and sites of interpretation, demonstrating the fit of model M8–3 for $Im(Z_{xy})$. The *rms* residual between empirical estimates (shown with their error bars) and modelling results (from the dashed theoretical curves) is 1.7 km.

PC5000 at 233 km) reveal a deep structure of extremely variable resistivity. Severe problems are encountered here to find stable solutions; the fit is poor in comparison to the central section. Forward calculations indicate that the inductive coupling between the deep anomalous structures beneath the three sections is weak, which justifies their separate treatment.

5.   Distribution of Individual Residuals

So far the outcome of 2D modelling has been rated on the size of the *mean* residual ϵ of Eq. (8). As a measure for the overall fit of a model it may conceal, however, trends and systematic tendencies of *individual* residuals, i.e., of the unexplained differences between an observed and a calculated datum. Assuming random data errors, these differences should also be randomly distributed. If not, the model is inadequate to explain certain significant aspects of the data.

Starting with the residuals of impedances Z_{xy}, Fig. 7 displays again their imaginary parts in the form of z^* depth estimates, now with error bars and in comparison to calculated values for a specific model. Both are shown only for the twenty sites whose data were used for modelling. The selected model is model M8–3 from a combined interpretation of MT and GDS data (cf. Table 3 and Fig. 9).

As seen from Fig. 7, the model produces smooth z^* curves which for the two long periods indeed follow closely the empirical estimates, passing often through them within error limits. For short periods, however, the estimates deviate in the center systematically from their predicted values. In particular, the reversal of the pronounced upward deflection of z^* at 683 s into a downward deflection at 85 s is not accounted for by the model. Models with more subdivisions do not lead to more randomly distributed residuals and similar observations apply to the not shown real parts of Z_{xy}. Hence, it appears that the model setup has an unresolved basic deficiency, as concluded already in the previous section from the size of the residual in comparison to the data errors.

This is exemplified by the distribution of various residuals in Fig. 8, representing the differences between the observed and calculated quantity after the last iteration. In the case of E_{ax} their distribution histograms are clearly non-symmetric with regard to zero deviation and the same applies to the phases which are systematically overestimated by the model. On the other hand, the residuals of apparent resistivities are distributed as if they were more or less normally distributed random variables. Therefore, the fit of the phases seems to be the problem which in turn spreads to the non-random behaviour of both the real and imaginary parts of E_{ax}.

Turning to the residuals of GDS data, Fig. 9 shows empirical estimates of B_{az} together with two theoretical curves, one for model M8 from MT data alone and one again for model M8–3. They demonstrate, how much better the observed magnetic variation anomaly can be explained, when GDS data are included in the 2D modelling process. In fact, model M8 yields only a fraction of the observed anomaly of B_{az}, but there remain substantial deviations between the observed and calculated B_{az} anomaly, in particular when the imaginary parts are considered (not shown).

It remains to examine how well the so far ignored MT data for B-polarisation can be explained. Figure 10 presents the relevant results from forward modelling with model M8–T*, which has the most finely subdivided top layer. Even though it cannot be expected that E-polarisation data yield the required details on surface resistivities, which largely determine the B-polarisation impedance, it is disappointing to note that the model predictions deviate strongly from the observations. The deep-seated low resistivity zone should depress apparent resistivities from −50 to +50 km and move the phases downward from −50 to 0 km and upward from 0 to 50 km. None of this is clearly observed and it is difficult to see how observations in E- and B-polarisation could be reconciled without involving them jointly into a 2D modelling process.
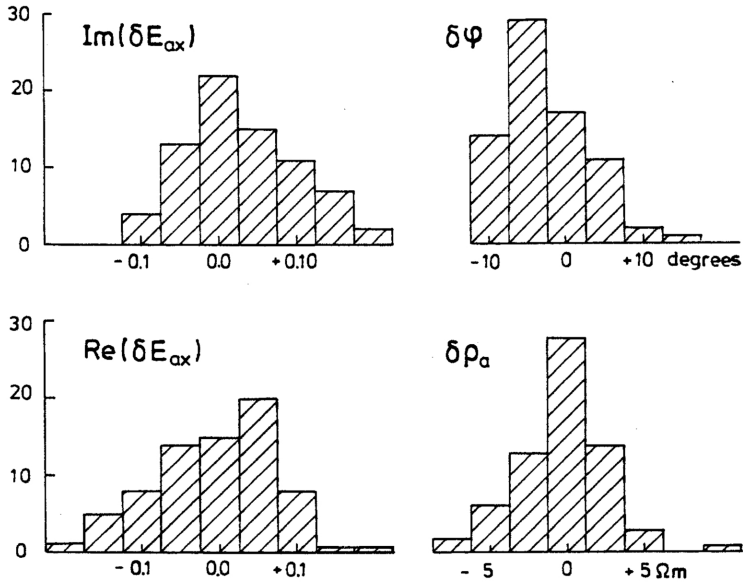
Fig. 8. Histograms of the $N = 148$ residuals of interpretation with model M8–3, revealing non-symmetries in the distribution of residuals for the anomalous electric field and the phase.
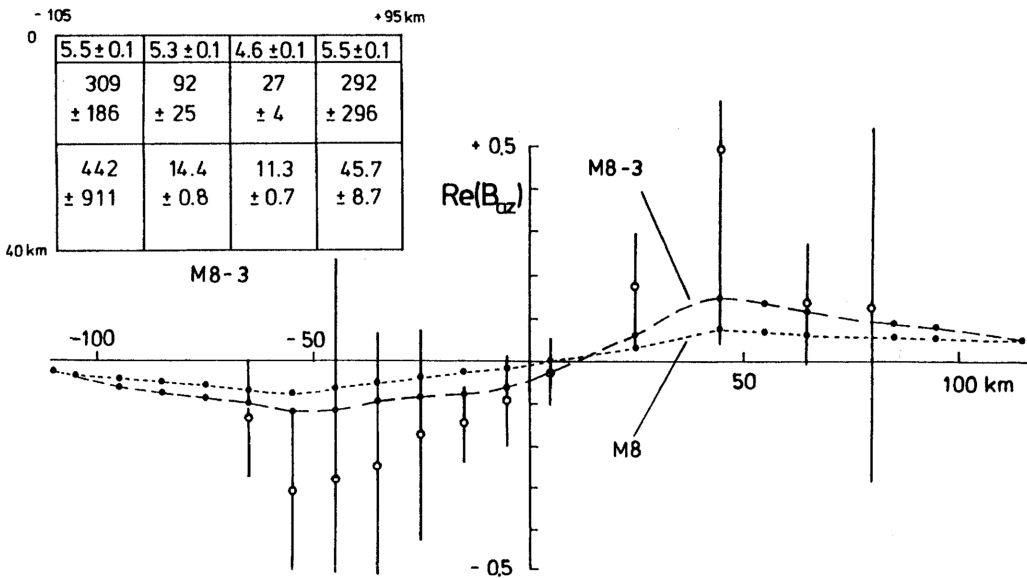

Fig. 9. In-phase magnetic variation anomaly B_{az} for $T = 683$ s. Empirical estimates at the twelve selected sites are compared to theoretical values for two models, model M8 as in Fig. 5 and model M8–3 as shown at the top left.
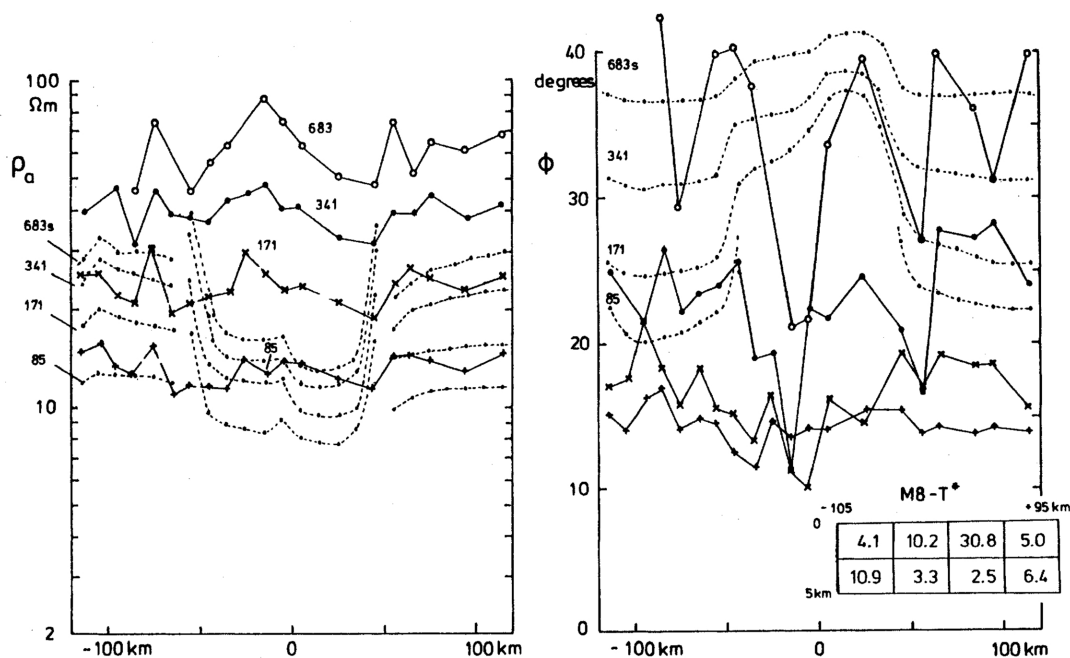
Fig. 10. *B*-polarisation apparent resistivities and phases for the periods and sites of interpretation with *E*-polarisation data. Empirical estimates are compared to theoretical values for model M8–D*, Table 4. The inset at the bottom right shows the resistivities of its top layers.

6.   Concluding Remarks

I see the advantage of the applied method of 2D modelling in the fact that by the use of linearized integral equations only the anomalous fields are interpreted. They are direct expressions of any anomalous conductivities within a prescribed anomalous domain. Model fit, model accuracy, and model resolution are well defined and can be used for deriving an optimum combination of them. However, the pragmatic way to avoid negative resistivities, by dampening of the solution, should be improved.

The drawback is that 1D modelling, which defines the reference normal structure, and 2D modelling do not interact. The mentioned possibility to remodel also the 1D reference in the course of the iterative 2D modelling process has not been used, but it seems unlikely that it could alter the outcome substantially. The problems lie elsewhere.

Firstly, it is not possible to find models which have residuals small enough to be comparable to the data errors (when only MT data for E-polarisation are used). It implies that even the reduced COPROD2 data set has not been exploited to its full possible extent. Secondly, the MT and GDS data are of uneven quality. It has been demonstrated, however, that their combined interpretation is essential. But in doing so, the residuals go down below the level set by the combined data errors, which are totally determined by those of the magnetic data. Hence, these combined data are overinterpreted. It should be remembered also that the GDS data could be included only after omitting the data of eight sites.

Models from a combined interpretation, such as model M8–3 in Fig. 9 or model M8–D* reproduced in JONES (1993), are considered as best describing the deep conductivity structure. Its main feature is a deep-seated low resistivity zone beneath the central sites where the resistivity

is reduced to 10 Ωm in comparison to more than 100 Ωm in the surrounding layers.

Thirdly, the inability to explain the B-polarisation data by these models is unresolved. Forward modelling studies show that the deep-seated low resistivity structure could be masked in B-polarisation by a highly non-uniform surface layer, but there is no evidence for that in the short period data. Even though a linearization of the integral equation for B-polarisation is possible and programs are ready to use them for 2D-modelling, not all numerical problems (which have to do with the all-important line integrations along subdomain boundaries) have been overcome. Future work may also concern the possibility to interpret data from both polarisations jointly, even though (for reasons given in Section 3) the approach with linearized integral equations meets here a fundamental limit.

REFERENCES

JONES, A. G., The COPROD2 dataset: Tectonic setting, recorded MT data and comparison of models, *J. Geomag. Geoelectr.*, this issue, 933–955, 1993.

LARSEN, J. C., Low frequency (0.1–6.0 cpd) electromagnetic study of deep mantle electrical conductivity beneath the Hawaiian islands, *Geophys. J. Roy. Astron. Soc.*, **43**, 17–46, 1975.

SCHMUCKER, U., Zur Modell(er)findung in 2D, in *Protokoll 14. Kolloquium Elektromagnetische Tiefenforschung Borkheide*, edited by V. Haak and H. Rodemann, pp. 3–18, Deutsche Geophysikalische Gesellschaft, 1992.

WEIDELT, P., *Entwicklung und Erprobung eines Verfahrens zur Inversion zweidimensionaler Leitfähigkeitsstrukturen in E-Polarisation*, Habilitationsschrift Univ. Göttingen, 1978.